Ultrafast far-infrared dynamics probed by terahertz pulses: a frequency domain approach. I. Model systems

H. Němec, F. Kadlec, S. Surendran, and P. Kužel*
Institute of Physics, Academy of Sciences of the Czech Republic, and Center for Complex Molecular Systems and Biomolecules Na Slovance 2, 182 21 Prague 8, Czech Republic

P. Jungwirth
Institute of Organic Chemistry and Biochemistry, Academy of Sciences of the Czech Republic, and Center for Complex Molecular Systems and Biomolecules Flemingovo nam. 2, 166 10 Prague 6, Czech Republic

Time-resolved terahertz spectroscopy has become a widely used experimental tool for the investigation of ultrafast dynamics of polar systems in the far infrared. We have recently proposed an analytical method for the extraction of a transient two-dimensional susceptibility from the experimental data [H. Němec et al., J. Chem. Phys. **117**, 8454 (2002)]. In the present paper the methodology of optical pump—terahertz probe experiments is further developed for direct application in realistic experimental situations. The expected two-dimensional transient response function is calculated for a number of model cases (including Drude dynamics of free carriers, harmonic and anharmonic oscillator modes); these results serve as a basis for the interpretation of experimental results. We discuss also the cases where only partial (one-dimensional) information about the system dynamics can be experimentally obtained.

I. INTRODUCTION

The fast development of the time-domain terahertz (THz) spectroscopy has enabled a widespread use of this technique as a sensitive probe of far-infrared response of polar systems in steady state[1,2]. This is mainly due to significant improvements of the signal-to-noise ratio and of the dynamic range of THz systems and due to the inherent possibility to analyze experimentally the THz electric field (and not only the power as in usual optical experiments). The experiments then provide directly the complex dielectric function of the sample without the need of data fitting or of Kramers-Kronig analysis. Furthermore, the technique of synchronous gated emission and detection of THz pulses along with the ability to resolve the electric-field profile of THz waveforms with a sub-picosecond resolution allow setting up time-resolved experiments of photo-excited media in the far-infrared. The term optical pump—THz probe (OPTP) is usually used for experiments in which the broadband THz pulses are used to probe changes of the far-infrared susceptibility (or conductivity) spectrum initiated by an optical excitation event (see Ref. 3 for a review).

Compared to the standard optical pump—optical probe (OPOP) spectroscopy the OPTP experiments differ in three aspects: (i) a different spectral range is probed; (ii) OPOP technique in the common setup measures time-resolved power reflectance or transmittance at carrier frequency of the probe pulse. The experimental results then provide a nonlinear susceptibility as a function of pump–probe delay, i.e. for a single experiment a real one-dimensional (1D) curve is accessed. In contrast, OPTP experiments are sensitive to the transient (time-resolved) THz electric field which depends on the pump-probe delay. Consequently, complex time-resolved THz spectra can be in principle obtained from a single experiment yielding a two-dimensional (2D) complex response function[4]. (iii) The time resolution in the OPTP experiments is not related to the THz pulse length (which extends typically over more than 1 ps); rather, it is limited by the bandwidth of the gated detection process which yields a sub-ps resolution (typically 0.3–0.4 ps). On the other hand, the investigated systems exhibiting picosecond or sub-picosecond dynamics involve frequency components falling into (or overlapping with) the THz range. This may produce a frequency mixing which distorts the transient THz waveform[5]. In other words, the leading and trailing parts of the THz pulse may probe the sample in two different states.

The two latter issues pointed out above lead to a conclusion that the OPTP experiments contain potentially more information, however, an appropriate care should be taken to extract this information correctly from the experimental data.

A number of papers have been devoted to the time-resolved THz studies of photo-carrier dynamics in semiconductors[6–10] and superconductors[11,12] and to charge transfer in photo-ionized liquids[13]. In these experiments the free carrier absorption represents the principal interaction of the THz radiation with the sample. A smaller number of papers have dealt with an experimentally challenging study of photo-induced environmental vibrational or librational response in solutions[14–18]. Clearly, if the rate of the probed dynamics exceeds tens of ps, no special treatment or methodology is required to obtain correct results. As to the investigation of faster dynamics, two different methodological approaches have been proposed up to now.

Historically the first approach, proposed by Schmut-

tenmaer and his group[16], is based on time-domain calculations and has been applied in several experimental works[10,17]. It uses the numerical method of finite-difference time-domain (FDTD) calculations which simulates the propagation of the THz pulse through the non-equilibrium medium with a known dielectric response. The advantage of this method is that it can take into account all non-equilibrium effects; in particular it can account for situations where the modifications of the THz field are strong and cannot be described using a perturbative approach. On the other hand, the FDTD method was not designed for the solution of the inverse problem, i.e., the extraction of the sought nonlinear susceptibility is not straightforward. The method requires *a priori* an explicit model for non-equilibrium behavior, the parameters of which are to be adjusted using FDTD calculations.

Recently, we have solved analytically the problem of propagation of broadband THz pulses in photo-excited media[5]. We have introduced a frequency-domain formalism which handles to the first order all non-equilibrium effects, including refraction on the surfaces of a photo-excited medium, dispersion, THz/optical velocity mismatch and pump intensity extinction. This treatment makes it possible to obtain the 2D nonlinear susceptibility in the frequency domain from the experimental data using explicit analytical formulae. It also provides strategies for carrying out the experiment in order to cancel or minimize the influence of instrumental functions of the THz setup. Nevertheless, an experimental demonstration of this approach which would show the ability of this method to find the unknown nonlinear susceptibility is still lacking. The aim of this paper is to fill this gap by a thorough experimental and theoretical study: we present experimental data for various physical and/or chemical systems exhibiting different behavior and we discuss the observed features in the nonlinear susceptibility and their interpretation.

The present paper reviews the principal results of our methodological approach (Sec. II) and it is mainly devoted to phenomenological modelling of 2D nonlinear susceptibility (Sec. III). The following paper in this issue[19] (Paper II) then shows experimental results obtained in semiconductors and molecular systems and provides their detailed treatment and interpretation within the frame of the developed models.

II. REVIEW OF THE FREQUENCY-DOMAIN APPROACH

The approach discussed in this section has been developed in Ref. 5 where the reader can find the details of underlying calculations. The aim of this section is to introduce the principal notions of our description of OPTP experiments, to present concisely the main findings and conclusions, and to provide a short reference for the experimentalists.

A. Transient THz field

The dynamics of a photo-excited system can be described by a nonlinear polarization ΔP introducing a 2D susceptibility $\Delta\chi$.[4,5] In many cases it is more suitable to use an equivalent treatment in terms of a non-equilibrium conductivity $\Delta\sigma$ and an induced electric current Δj:

$$\Delta j(t-t_p, t-t_e) = \int_{-\infty}^{t} E_{\mathrm{THz}}(t'-t_p)\,\Delta\sigma(t-t', t-t_e)\,dt' \tag{1}$$

where t_e marks the time of the optical excitation, t_p is connected to THz probe pulse arrival, and t defines the time of the measurement (i.e. the real time). In the experiment, the arrival of the pulses is controlled by delay lines D1, D2 and D3, respectively (see Figure 1). The photo-induced transient conductivity $\Delta\sigma$ is proportional to the pump pulse intensity and depends on two time variables: the first one is related to the dielectric response to the probe pulse, and the second one describes the influence of the optical excitation. The field E_{THz} in the sample consists of the equilibrium part E_0 and of a small transient part ΔE which is generated by the nonlinear current Δj.

When a 2D scan is performed, two delay lines are moving and the remaining one is held in a fixed position. We have shown[5] that two cases (representations) should be considered:
(I) D3, which determines time t, is fixed; we define two independent variables for the time scans: $\tau_e = t - t_e$ (controlled by D1) and $\tau = t - t_p$ (D2) with the conjugated frequency-domain variables ω_e and ω.
(II) D2, which determines time t_p, is fixed; the time-domain variables are: $\tau_p = t_p - t_e$ (D1) and $\tau = t - t_p$ (D3); the frequency-domain variables are: ω_p and ω.

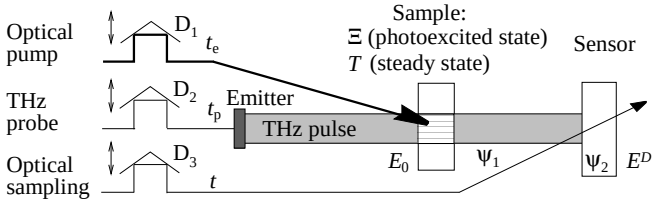

FIG. 1: Scheme of OPTP technique. For definition of symbols, see text.

In the following text, the 2D physical quantities labeled by the superscript (I) are expressed by means of variables τ_e and τ or ω_e and ω (i.e., inherent variables of representation I) and quantities labeled by the superscript (II) are expressed through τ_p and τ or ω_p and ω (i.e., inherent variables of representation II). We would like to stress that a relevant physical quantity (e.g. $\Delta\sigma^{(\mathrm{I})}$ and $\Delta\sigma^{(\mathrm{II})}$) can be expressed in either representation while it always describes the same physical process. In this sense, on one hand, both representations of the chosen quantity are equivalent, i.e., they contain the same information

about the system. On the other hand, their mathematical form is different as they are expressed using different inherent variables. In addition, they can be accessed using different experimental protocols and, as it is pointed out below, the frequency domain quantities are obtained by a different transformation of the experimental data.

One can easily show[5] that in the time domain

$$\Delta\sigma^{(\mathrm{I})}(\tau,\tau_e)=\Delta\sigma^{(\mathrm{II})}(\tau,\tau_p=\tau_e-\tau) \tag{2}$$

and in the frequency domain

$$\Delta\sigma^{(\mathrm{I})}(\omega,\omega_e)=\Delta\sigma^{(\mathrm{II})}(\omega+\omega_e\to\omega,\omega_e\to\omega_p)\,, \tag{3}$$

which means that upon passing from representation I to representation II ($\omega+\omega_e$) is replaced by ω and ω_e is replaced by ω_p.

The wave equation describing propagation of the electromagnetic field in the photo-excited medium can be solved analytically in the Fourier space[5] within the approximation $\Delta E \ll E_0$. One finds for the outgoing transient part of the THz field in representation I:

$$\Delta E^{(\mathrm{I})}(\omega,\omega_e)=\frac{\Delta\sigma^{(\mathrm{I})}(\omega,\omega_e)}{i\,(\omega+\omega_e)\,\varepsilon_0}\;\Xi^{(\mathrm{I})}(\omega+\omega_e,\omega)E_0(\omega)\,, \tag{4}$$

and in representation II:

$$\Delta E^{(\mathrm{II})}(\omega,\omega_p)=\frac{\Delta\sigma^{(\mathrm{II})}(\omega,\omega_p)}{i\,\omega\,\varepsilon_0}\;\Xi^{(\mathrm{II})}(\omega,\omega-\omega_p)E_0(\omega-\omega_p)\,, \tag{5}$$

where $\Xi^{(\mathrm{I,II})}$, introduced by Eqs. (30) and (31) in Ref. 5, is a transfer function of the photo-excited sample. This function depends on the THz dispersion of the sample in equilibrium, on its optical absorption coefficient and group velocity, and on its thickness. It can be unambiguously determined from a steady-state experiment. In the general case the form of $\Xi^{(\mathrm{I,II})}$ can be complicated; on the other hand, it can be easily shown that in the most interesting experimental cases $\Xi^{(\mathrm{I,II})}$ takes a rather simple form. For the analysis of the experimental results we always use the general formula for Ξ, however, it is worth inspecting its behavior in the simple cases.

Let us assume for a while that the THz dispersion of the sample in equilibrium is negligible. It then follows from Ref. 5 [see Eqs. (33) and (34) therein] that both in the case of a bulk phase-matched interaction and in the case of a high optical absorption of the sample (i.e., the case encountered often in semiconductors where the OPTP signal is mainly generated at the input face of the sample):

$$\Xi^{(\mathrm{I})} \;\propto\; i(\omega+\omega_e)\,, \tag{6}$$

$$\Xi^{(\mathrm{II})} \;\propto\; i\omega\,. \tag{7}$$

This simplified approach immediately yields:

$$\Delta E^{(\mathrm{I})}(\tau,\tau_e) \;\propto\; \Delta j^{(\mathrm{I})}(\tau,\tau_e)\,, \tag{8}$$

$$\Delta E^{(\mathrm{II})}(\tau,\tau_p) \;\propto\; \Delta j^{(\mathrm{II})}(\tau,\tau_p)\,. \tag{9}$$

We return back to the general case. Note that the quantity ΔE is not directly measured: it represents the transient field just leaving the sample (near field). The detected transient signal is obtained using the convolution theorem [cf. Eqs. (12a,b) in Ref. 5]:
Representation I:

$$\Delta E^{D,(\mathrm{I})}(\omega,\omega_e)=\psi_2(\omega+\omega_e)\psi_1(\omega+\omega_e)\Delta E^{(\mathrm{I})}(\omega,\omega_e)\,, \tag{10}$$

Representation II:

$$\Delta E^{D,(\mathrm{II})}(\omega,\omega_p)=\psi_2(\omega)\psi_1(\omega)\Delta E^{(\mathrm{II})}(\omega,\omega_p)\,, \tag{11}$$

where ψ_1 and ψ_2 are the instrumental functions describing the propagation of the THz pulse between the sample and the sensor and the response of the sensor, respectively (see Figure 1).

A reference measurement in the pump-probe studies is obtained in equilibrium (i.e., without the optical pump). The detected reference waveform transmitted through the optically unexcited sample reads:

$$E^{D}_{\mathrm{ref}}(\omega)=\psi_2(\omega)\psi_1(\omega)T(\omega)E_0(\omega)\,, \tag{12}$$

where T is the complex equilibrium transmission function of the sample.

Eqs. (4), (10) and (12)—for representation I, and (5), (11) and (12)—for representation II, constitute the basis for the experimental determination of $\Delta\sigma$. Their thorough understanding requires a short discussion.

B. Representation I

In this experimental scheme one varies the delays D1 (scan of t_e) and D2 (scan of t_p), while the time t (D3) is fixed. For a given position of D1 (fixed excitation event) a waveform scan is realized using D2. This implies that one cannot access a single propagating THz waveform (which is connected to the time t). Instead, one collects data points from different transient THz pulses all measured with the same time distance between the pump and the gated detection event. We can still call the measured curve a waveform, however, it is important to realize that it does not exist in real time but it is connected to time t_p. In the detection process, though, the response function of the sensor is always convoluted with waveforms existing in real time. The direct consequence of this fact is that the detection process and the propagation between the sample and the sensor involve frequency mixing in terms of $\omega+\omega_e$.

Thus the experimentally obtained ratio

$$\frac{\Delta E^{D,(\mathrm{I})}(\omega,\omega_e)}{E^{D}_{\mathrm{ref}}(\omega)}$$

does not allow for canceling out the instrumental functions. It is necessary to know the sensor response function ψ_2 defined, e.g., by Eq. (38) in Ref. 5. It is also

required to simplify the optical path of the THz pulses between the sample and the sensor as much as possible so as to enable the determination of ψ_1. It has been suggested[5] that the experiments should be carried out in the far-field (without any transformation of the THz beam between the sample and the sensor) to obtain plausible experimental data.

C. Representation II

Using this experimental protocol a 2D scan is realized through D1 (scan of t_e) and D3 (scan of t). By contrast with the preceding scheme, a D3-scan with a fixed position of D1 directly yields a single propagating transient THz waveform induced by the pump pulse. The convolution with the instrumental functions (11) is then simplified as expected. However, different points on the THz waveform experience a different delay with respect to the excitation event, leading to the frequency mixing between the incident THz waveform $E_0(\omega - \omega_p)$ and the transient signal $\Delta E^{(\mathrm{II})}(\omega, \omega_p)$.

The determination of the transient conductivity from the ratio

$$\frac{\Delta E^{D,(\mathrm{II})}(\omega, \omega_p)}{E^D_{\mathrm{ref}}(\omega)}$$

therefore requires knowledge of the shape of the THz waveform incident on the sample. This implies replacing the sample by the sensor, measuring the waveform and, subsequently, its deconvolution with the sensor response function ψ_2.

The protocol related to representation II thus requires an additional measurement compared to that related to representation I. This is counterbalanced by the fact that representation II allows one to choose the most suitable experimental arrangement behind the sample from the point of view of the signal-to-noise ratio, namely, to focus the THz beam into the sensor. Note also that the knowledge of the sensor response function is required in both schemes. This response always involves frequency mixing: $\psi_2(\omega + \omega_e)$ in representation I and $\psi_2(\omega - \omega_p)$ in representation II.

D. Accessible spectral range

The nonlinear conductivity (or susceptibility) can be experimentally determined only in the spectral ranges where both ΔE^D and E^D_{ref} are non-vanishing and exceed the noise level. Clearly, owing to frequency mixing, the accessible region in the 2D (ω, ω_e) or (ω, ω_p) space is not rectangular but it is a union of several polygons (see Figure 6 in Ref. 5). In fact, the terms which contain the argument $\omega + \omega_e$ or the argument $\omega - \omega_p$ are at the origin of diagonal spectral delimiters. The most important factor is related to the upper limit of the spectral sensitivity of the sensor which, due to its diagonal character, significantly reduces the experimentally accessible area. For a typical THz experiment based on a ZnTe emitter and sensor, one obtains $|\omega|$, $|\omega_e + \omega|$, $|\omega - \omega_p| < 2.5$ THz.

This discussion reveals the advantage of the frequency domain approach. A careful analysis of the experiment unambiguously yields the spectral region where the transient conductivity can be obtained; the experimental error can be also quantified in this region. Up to this point no *a priori* information about the dynamics of the system under investigation is needed. It also follows that any time-domain representation of the conductivity is more or less distorted and/or it should be based on some model assumptions about the system studied.

The experimentalist obtains a 2D "map" of the transient complex conductivity expressed in the frequency space which provides a macroscopic picture of ultrafast dynamics of charges; he should then decrypt it and assign to underlying processes. This can be performed on a microscopic scale using, e.g., molecular dynamics simulations, or within a phenomenological macroscopic framework. In this paper we use the latter approach to find the expected form of the transient conductivity in simple model situations for several qualitatively different types of response. Paper II then supplements this theoretical work with data taken for several experimentally interesting systems.

III. MODELS FOR TRANSIENT CONDUCTIVITY

A. General considerations

For simplicity we assume in this section that the optical pump pulse excites only one kind of quasi-particles (e.g. free electrons in semiconductors, vibrational or librational mode in a molecular crystal or in a solution etc.); a generalization of this model is straightforward. Furthermore, we assume a local character of the response both to the optical and THz pulses. Let the indices G and E denote the properties of particles in the ground and optically excited state, respectively. The macroscopic current in the sample is given by the mean velocity calculated by averaging individual velocities v_i of charged particles:

$$j(t) = q \sum v_i(t) = q\, n\, \langle v(t) \rangle \,, \tag{13}$$

where n is the number of particles and q is their charge. The transient photo-current then reads:

$$\Delta j(t, t_e) = q\, n\, \left[\langle v(t, t_e) \rangle_E - \langle v(t) \rangle_G \right] . \tag{14}$$

On one hand the transient velocities can be extracted from molecular dynamics simulations[18]. Such an approach has the advantage of obtaining a detailed dynamical picture with molecular resolution, provided a reliable atom-atom interaction potential is available. The main drawback of this direct approach is that the response of

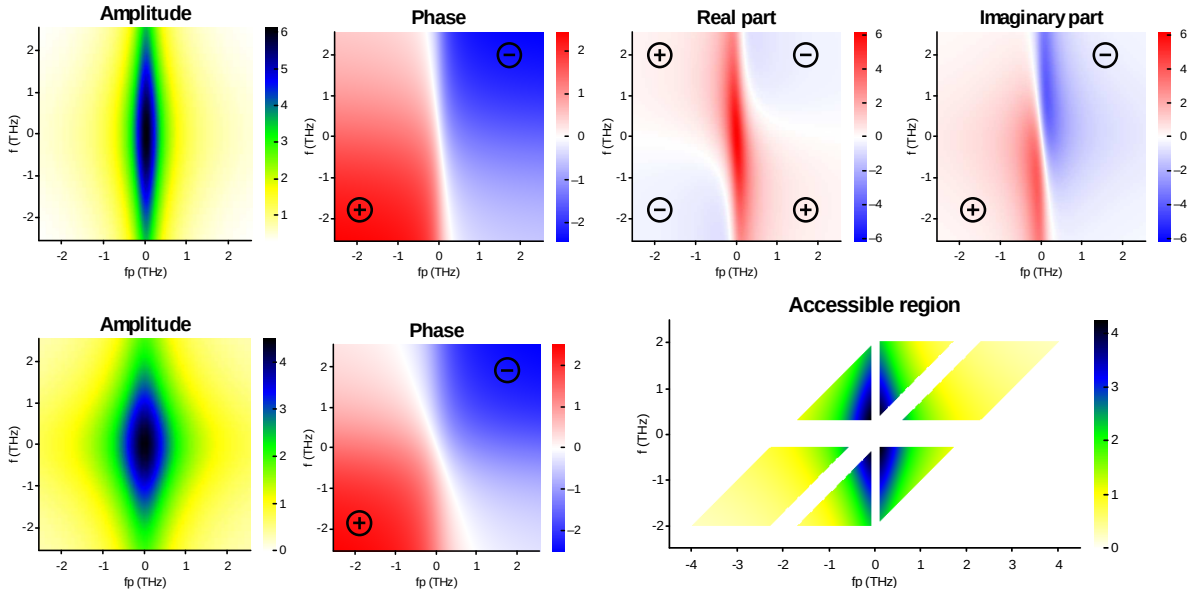

FIG. 2: Simulations of transient 2D conductivity $\Delta\sigma^{(\mathrm{II})}(\omega,\omega_p)$ for free carrier dynamics following (31). Upper row: $\tau_c = 0.7$ ps, $\tau_s = 0.1$ ps; lower row: $\tau_c = 0.35$ ps, $\tau_s = 0.2$ ps. The rightmost plot in the lower row shows a typical accessible area using the available spectral range of 300 GHz–2 THz.

the system to the THz probe pulse is very weak (unlike the response to the optical pump pulse) and it tends to be buried in the statistical noise inherent to simulations with a finite number of particles. On the other hand, it is also possible to develop a macroscopic phenomenological model describing the average particle position $x(t,t_e)$ and velocity $\dot{x}(t,t_e)$. One can introduce time-dependent velocity distribution functions $p_{E,G}(t,t_e)$:

$$\langle v(t,t_e)\rangle_{E,G} = \int p_{E,G}(t,t_e)\, v\, dv\,. \tag{15}$$

The model assumption then consists in the possibility of factorization of this distribution function:

$$\begin{aligned} p_E(t,t_e) &= \rho(t-t_e)\,\delta(v-\dot{x}_E(t,t_e)) \\ &+ [1-\rho(t-t_e)]\,\delta(v-\dot{x}_G(t))\,, \qquad (16)\\ p_G(t) &= \delta(v-\dot{x}_G(t))\,, \qquad (17)\end{aligned}$$

where $x_E(t,t_e)$ and $x_G(t)$ are solutions of a model set of equations of motion which should be supplied to describe the motion of charges (either free or bound) in the excited and ground state, respectively; δ denotes the Dirac δ-function. The function $\rho(t-t_e)$ then can be interpreted in terms of the variation of the excited state population.

The coupling constant to the THz probe field (effective charge) is denoted by $f_{E,G}$; for sake of generality we assume that it can be time dependent. The photo-induced current is then equal to:

$$\Delta j(t,t-t_e) = n_E(t-t_e)[f_E(t-t_e)\dot{x}_E(t,t-t_e) - f_G\dot{x}_G(t)]\,. \tag{18}$$

In our model, the density of excited particles n_E does not depend on the THz probe field and it obeys a differential equation with the optical delta-pulse representing the source term:

$$D(t)n_E(t-t_e) = n_0\delta(t-t_e)\,, \tag{19}$$

where D is a differential operator describing the depopulation of the excited state and n_0 is the density of photocarriers immediately after excitation.

The dynamical response of the system in equilibrium to the THz probe field E_0 can be described by a differential operator L_G:

$$L_G(t)x_G(t) = f_G E_0(t)\,. \tag{20}$$

One obtains in terms of a Green's function:

$$L_G(t)G_G(t-t') = \delta(t-t')\,. \tag{21}$$

Out of equilibrium, the quasi-particle dynamics is described by a differential operator $L_E(t,t-t_e)$ and by the coupling function $f_E(t-t_e)$:

$$L_E(t,t-t_e)x_E(t,t-t_e) = f_E(t-t_e)E_0(t)\,; \tag{22}$$

using Green's function formalism, one finds:

$$L_E(t,t-t_e)G_E(t-t',t-t_e) = \delta(t-t')\,. \tag{23}$$

Explicit forms of operators D, L_G and L_E are discussed in the model applications below.

It can be now easily shown that the general form of the non-equilibrium current reads:

$$\Delta j(t,t-t_e) = n_E(t-t_e)\Big[f_E(t-t_e)\int_{-\infty}^{\infty} dt' f_E(t'-t_e)\dot{G}_E(t-t',t-t_e)E_0(t') - f_G^2\int_{-\infty}^{\infty} dt'\dot{G}_G(t-t')E_0(t')\Big], \quad (24)$$

where the causality is formally achieved by the Heaviside function $Y(t)$ which will be explicitly included in the Green's functions. Now, similarly as in Ref. 5, we can introduce the probe arrival time t_p and switch to the time delay variables. In representation I the non-equilibrium response function reads:

$$\Delta\sigma^{(\mathrm{I})}(\tau,\tau_e) = n_E(\tau_e)[f_E(\tau_e)f_E(\tau_e-\tau)\dot{G}_E(\tau,\tau_e) - f_G^2\dot{G}_G(\tau)]\,. \quad (25)$$

The simplest approximation for the behavior of the excited particles population n_E is a single exponential decay:

$$n_E(\tau_e) = n_0\, Y(\tau_e)\, \exp[-\tau_e/\tau_c]\,. \quad (26)$$

where τ_c is the particle lifetime in the excited state.

A special attention should be paid to the situation when the THz probe pulse arrives before the optical pump (i.e. $t_p < t_e$ or $\tau_p < 0$). We recall that t_p is connected to the arrival of the THz probe pulse. Consequently, in a real experiment, the origin of t_p is chosen to some extent arbitrarily given the temporal length of the THz pulse. However, regarding the transient conductivity as a response function to an impulsional probing field, t_p is unambiguously determined by the position of the probe δ-pulse. Thus, between t_p and t_e the system exhibits a dynamics described by G_G and driven by the THz field. At t_e the pump pulse optically excites the system. The physical state we probe after the photoexcitation may differ depending on the extent to which the phase and the amplitude of the equilibrium motion have been conserved on the timescale comparable to the upper frequency limit of the THz resolution. Strictly speaking, the initial conditions for the Green's function of the excited state read: $G_E(t=t_e) = G_G(t=t_e)$, $\dot{G}_E(t=t_e) = \dot{G}_G(t=t_e)$. However, in some cases, the position and the velocity of the particles can be changed on very short time scales due to efficient fast scattering mechanisms. A fast and efficient averaging of these quantities leads to a simpler initial condition $G_E(t=t_e) = \dot{G}_E(t=t_e) = 0$. In the following we will refer to these cases as to weakly perturbed systems described by the former initial conditions and we will call strongly perturbed systems those satisfying the latter ones. The latter condition can be also applied, e.g., to the case of optical interband excitation of semiconductors, where the motion of valence electrons is negligible compared to that of the conduction electrons ($G_G \ll G_E$).

In our model we consider explicitly that the coupling constant f_E may exhibit some dynamics upon photoexcitation. Furthermore, its time dependence provides a convenient way to "switch on" the interaction of the probe field with newly generated particles if we assume $f_E(t-t_e) \propto Y(t-t_e)$.

The 2D maps of the conductivity we discuss in the following paragraphs are essentially based on Eq. (25) using some model behavior of the excitations. We discuss several cases including the Drude model of free carriers and oscillatory behavior of bound charges. In this paper, we derive the behavior of the transient susceptibility for the model cases and discuss what can then be obtained by OPTP experiments. In Paper II, the relevance of these models for particular physical situations is addressed.

B. Drude dynamics and trapping of free carriers

This case covers a broad class of applications of OPTP experiments to systems in which carriers can be excited by an optical pump pulse to states described by a delocalized wave function, i.e., the restoring force is absent. It concerns namely semiconductors with ultrafast response like low-temperature grown GaAs (LT-GaAs)[20], radiation-damaged silicon-on-sapphire (RD-SOS)[21], low-temperature grown InAlAs[22], etc. This model can also describe to a large extent the dynamics of carriers after multi-photon ionization in fluids[13].

1. 2D scans

The kinetic equations read[23]:

$$\frac{dn_E}{dt} + \frac{n_E}{\tau_c} = n_0\delta(t-t_e) \quad (27)$$

$$m\frac{d^2x_E}{dt^2} + \frac{m}{\tau_s}\frac{dx_E}{dt} = qY(t-t_e)E_0(t)\,. \quad (28)$$

where τ_c is the lifetime of free carriers and τ_s is their momentum scattering time. We assume immobile valence electrons. The equations yield the following dynamical parameters:

$$\begin{aligned} n_E &= n_0\, Y(t-t_e)\, \exp[-(t-t_e)/\tau_c]\,,\\ f_G &= 0\,,\\ \dot{G}_G &= 0\,,\\ f_E(t-t_e) &= q\,Y(t-t_e)\,,\\ \dot{G}_E(t,t-t_e) &= Y(t-t_e)Y(t)/m\, \exp(-t/\tau_s)\,. \end{aligned}$$

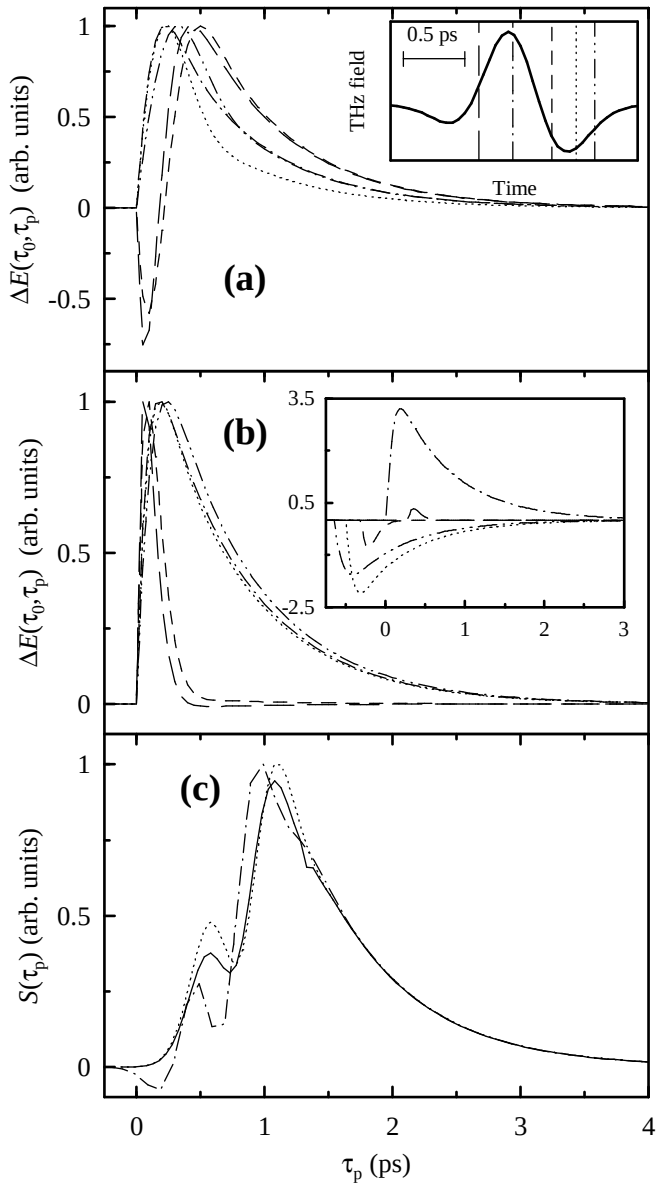

FIG. 3: Simulations of 1D pump–probe scans for free carrier dynamics. Inset of (a): The shape of the THz waveform $E_0(t)$ used in the calculations. (a), (b): Signal (normalized to unity and shifted to the common time origin) for a pump–probe scan at a fixed waveform position ($\tau = \tau_0$) based on Eq. (36); the lines correspond to different waveform positions (τ_0) indicated in the inset of (a): the motifs of lines mutually correspond. Parameters: $\tau_c = 0.7$ ps, $\tau_s = 0.25$ ps (a), $\tau_s = 0.1$ ps (b). Inset of (b): the same signal as in (b) but not normalized to unity and not shifted. (c): Normalized signal for a pump–probe scan using a time-integrating detector. Parameters: $\tau_c = 0.7$ ps, full line ($\tau_s = 0.1$ ps, near field), dotted line ($\tau_s = 0.25$ ps, near field), dash-dotted line ($\tau_s = 0.25$ ps, far field).

The transient response function then reads:

$$\Delta\sigma^{(\mathrm{I})}(\tau,\tau_e) = \frac{q^2 n_0}{m} Y(\tau) Y(\tau_e - \tau) \exp(-\tau_e/\tau_c) \exp(-\tau/\tau_s)\,. \tag{29}$$

The 2D Fourier transform is straightforward and easy to perform:

$$\Delta\sigma^{(\mathrm{I})}(\omega,\omega_e) \;=\; \frac{B}{i(\omega+\omega_e)+1/\tau_f}\,\frac{1}{i\omega_e+1/\tau_c}\,, \tag{30}$$

$$\Delta\sigma^{(\mathrm{II})}(\omega,\omega_p) \;=\; \frac{B}{i\omega+1/\tau_f}\,\frac{1}{i\omega_p+1/\tau_c}\,. \tag{31}$$

with

$$\frac{1}{\tau_f} \;=\; \frac{1}{\tau_c}+\frac{1}{\tau_s}\,, \tag{32}$$

$$B \;=\; \frac{q^2 n_0}{m}\,. \tag{33}$$

The transient conductivity shows a single pole at the origin of frequency axes and its amplitude decreases with increasing frequencies; the speed of this decrease is a measure of τ_c and τ_s (see Figure 2). For these plots the upper limit of 2.5 THz of the sensor spectral sensitivity was used. Note that the scattering time of 100 fs can be still resolved in such data. Indeed, the use of 2D complex fitting makes it possible to determine time constants as fast as 50 fs assuming still the 2.5 THz upper detection limit. Note also that even shorter time constants can be determined if the parameter B can be independently estimated from the experiment.

By performing a 1D inverse Fourier transform in ω_p (frequency conjugated to the pump–probe delay τ_p) one obtains in representation II a simple expression:

$$\Delta\sigma^{(\mathrm{II})}(\omega,\tau_p) = \frac{B}{i\omega+1/\tau_f}\,Y(\tau_p)\,\exp(-\tau_p/\tau_c)\,. \tag{34}$$

This formula can be interpreted in terms of a series of THz snapshots with a single exponential decay due to the carrier trapping. For any pump–probe delay the individual THz spectra show a Drude-like shape characterized by a time constant τ_f which is a combination of the decay and scattering times.

We stress once more that experimentally such data cannot be obtained directly by a 1D Fourier transformation of the measured ratio $\Delta E^D(\tau,\tau_p)/E^D_{\mathrm{ref}}(\tau)$. The passage through the 2D Fourier space and the appropriate data transformation are required.

The transient current can be also calculated; it depends in a rather complicated way on a particular THz waveform:

$$\Delta j^{(\mathrm{II})}(\omega,\tau_p) \propto \frac{\exp(-\tau_p/\tau_c)}{i\omega+1/\tau_f} \int\limits_{-\tau_p}^{\infty} dt' \exp[-t'(i\omega+1/\tau_c)] E_0(t')\,. \tag{35}$$

2. 1D pump–probe scans

In some OPTP studies the authors have performed 1D scans only to obtain dynamical information. This strategy is required for systems where the THz transient signal is extremely week and 2D scans can be hardly performed. Two different types of 1D scans have been used so far. (i) The delay between the THz probe and the optical gating pulse is held constant (i.e. τ is fixed) while the advance of the pump pulse is changed during the experiment[15,24,25]; (ii) A THz power detector (e.g. a bolometer) is used instead of a gated detection scheme; the whole THz power is then detected as a function of pump probe delay[14,26]. In both cases τ_p is scanned.

The present model of the dynamics of free carriers provides analytical expressions for all quantities of interest. Thus it can also serve as a simple tool to analyze 1D experiments. To simplify this short analysis, let us adopt the assumptions which lead to expressions (8) and (9). In addition we assume here a flat spectral response of the THz detectors.

Eq. (24) applied to our model then leads to the expression for the near-field transient waveform:

$$\Delta E(\tau,\tau_p) \propto \exp(-\tau_p/\tau_c) Y(\tau+\tau_p) \exp(-\tau/\tau_c) \int_0^{\tau+\tau_p} dt' E_0(\tau-t') \exp(-t'/\tau_s)\,. \tag{36}$$

In the case of the pump–probe scan of a THz field at a fixed waveform position $\tau = \tau_0$, the observed quantity is proportional to:

$$\Delta E^D(\tau_0,\tau_p) \propto \int_{-\infty}^{\infty} dt' \psi_1(t') \Delta E(\tau_0 - t', \tau_p)\,. \tag{37}$$

In the case of the pump–probe scan with a time integrating detector the measured signal is proportional to:

$$\begin{aligned} S(\tau_p) \;\propto\; & \int_{-\infty}^{\infty} dt' \psi_1(t') \int_{-\infty}^{\infty} dt'' \psi_1(t'') \\ & \times \int_{-\infty}^{\infty} d\tau \Delta E(\tau - t', \tau_p) E_0(\tau - t'')\,. \end{aligned} \tag{38}$$

$\psi_1(t)$ is the instrumental function describing the propagation of THz waveforms between the sample and the detector. In the simplest cases $\psi_1(t) = \delta(t)$ or $\psi_1(t) = \delta'(t)$ (derivative of the Dirac δ-function) for the measurement in the near- or far-field, respectively. In the case of focusing by a mirror or a lens with a finite aperture, and with the object/image size ratio 1:1, a useful approximation is represented by (see Ref. 27 for details):

$$\psi_1(t) = \delta(t) - \sqrt{\frac{\alpha}{\pi}}\, \exp(-\alpha t^2)\,.$$

Examples of the observables for the two experiments are shown in Figure 3. We assumed here the simplest case of the measurement in the near field, i.e., Eq. (36) and

$$\begin{aligned} S(\tau_p) \;\propto\; & \exp(-\tau_p/\tau_c) \int_{-\tau_p}^{\infty} d\tau E_0(\tau) \exp(-\tau/\tau_c) \\ & \times \int_0^{\tau+\tau_p} dt' \exp(-t'/\tau_s) E_0(\tau - t')\,. \end{aligned} \tag{39}$$

The following conclusions can be deduced from the simulations. If there is a measurable signal for delays larger than approximately the THz probe pulse length ($\sim$1 ps in our simulations), the fitting of this part of the signal by a single exponential always yields the correct trapping time τ_c. Extending the fitting range towards shorter delays may lead to incorrect results. The data corresponding to short pump–probe delays cannot be analyzed in a simple way. The signal in this range depends on the incident THz waveform, on the momentum scattering rate and on the experimental setup (using different instrumental functions ψ_1 leads to qualitatively similar but quantitatively very different curves). For example, the oscillations in the signal shown in Figures 3a,c are not caused by an oscillatory behavior of the studied system; rather, they are a consequence of particular experimental conditions and parameters. These findings will be also experimentally demonstrated in Paper II.

In summary, results obtained for an unknown physical system using 1D pump–probe scans should be analyzed very carefully. Despite of a presumed higher temporal resolution of the experiments, safely correct results are obtained only for delays exceeding the THz pulse length.

3. 1D transient waveform scans

In some dynamical studies another kind of 1D THz experiments can be useful. In this case the pump–probe delay is held at a fixed position τ_p and the transient THz waveform is recorded. In a large number of experimental works the transient THz waveforms are recorded for several values of τ_p, but not enough to provide a complete 2D picture[11,13,26]. The interpretation is then based on the behavior of Fourier transform of the recorded signal usually called transient THz spectra: typically, in the systems with free carriers, these spectra are fitted to the Drude formula.

Assuming the applicability of expressions (8) and (9) and using Eq. (35) we can easily find the form of the signal which is to be interpreted:

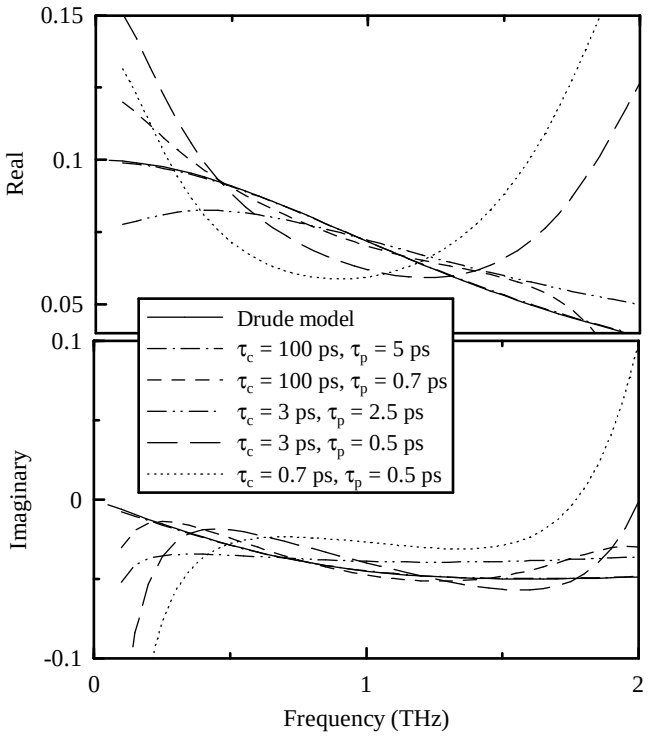

FIG. 4: Simulations of 1D transient waveform scans for free carrier dynamics. The transient THz spectra defined by Eq. (40) are plotted without taking into account the first exponential term. Momentum scattering time: $\tau_s = 0.1$ ps. Values of τ_p and τ_c are indicated in the legend. The Drude model corresponds to the situation when $\tau_p \to \infty$ and $\tau_c \to \infty$. Waveform shown in the inset of Figure 3a was used.

$$\frac{\Delta E^D(\omega,\tau_p)}{E^D_{\rm ref}(\omega)} \propto \frac{\exp(-\tau_p/\tau_c)}{i\omega+1/\tau_f}\,\frac{\int\limits_{-\tau_p}^{\infty} dt'\exp[-t'(i\omega+1/\tau_c)]\,E_0(t')}{\int\limits_{-\infty}^{\infty} dt'\exp(-i\omega t')\,E_0(t')}\,. \tag{40}$$

Consequently, the data exhibit necessarily a departure from the Drude behavior [even if, as in our model case, the physical process exactly follows the Drude dynamics expressed by Eq. (34)] in the case when (i) the trapping time is short (shorter than or comparable to the THz probe pulse length and/or the momentum scattering time τ_s) and (ii) the probe pulse comes too early after the pump (their time separation is shorter than the THz pulse length). These results are illustrated for several sets of dynamical parameters in Figure 4.

C. Harmonic oscillators: excitation of a vibrational mode

This paragraph deals with the case in which the eigenfrequency of a vibrational or librational mode changes upon photo-excitation. This type of dynamics can occur namely in molecular systems. For example, in the solvation dynamics experiments the photo-excitation of a chromophore in the solution, which is connected to the redistribution of charges, may cause a change of the interaction potential for an environmental mode of the first solvation layer[17]. In this paragraph we investigate the dynamics of such a system in the damped harmonic approximation. The equations of motion then read:

$$m\frac{d^2x_i}{dt^2} + m\gamma_i\frac{dx_i}{dt} + m\omega_i^2 x_i = f_i E_0(t)\,, \qquad (41)$$

where $i = E, G$ denotes coordinates and parameters of excited and ground state, respectively. We assume that, prior to the optical excitation, only oscillators with eigenfrequency ω_G and damping γ_G exist. Upon excitation some of these oscillators change their parameters to ω_E and γ_E. The population of excited-state oscillators may then exhibit a decay in time leading back to their ground-state characteristics. The oscillations occur at the reduced frequencies Ω_G and Ω_E:

$$\Omega_i = \sqrt{\omega_i^2 - \gamma_i^2/4}\,. \qquad (42)$$

We obtain:

$$\begin{aligned} n_E(\tau_e) &= n_0\, Y(\tau_e)\, \exp(-\tau_e/\tau_c)\,, \\ f_G &= q\,, \\ G_G(\tau) &= \frac{Y(\tau)}{m\Omega_G}\, \exp(-\gamma_G\tau/2)\, \sin(\Omega_G\tau)\,. \end{aligned}$$

In the case when during photo-excitation the system looses the motion information due to some fast scattering mechanisms [strongly perturbed systems: $G_E(\tau_e = 0) = \dot{G}_E(\tau_e = 0) = 0$] we get:

$$\begin{aligned} f_E(\tau_e) &= q\, Y(\tau_e)\,, \\ G_{E,0}(\tau) &= \frac{Y(\tau_e)Y(\tau)}{m\Omega_E}\, \exp(-\gamma_E\tau/2)\, \sin(\Omega_E\tau)\,, \end{aligned}$$

leading to

$$\Delta\sigma^{(\mathrm{I})}(\tau,\tau_e) = n_0 q^2 Y(\tau_e)\exp(-\tau_e/\tau_c)[Y(\tau_e-\tau)\dot{G}_{E,0}(\tau) - \dot{G}_G(\tau)]\,. \qquad (43)$$

In the case when the excited quasi-particles keep the position and velocity information of the ground-state [weakly perturbed systems: $G_E(\tau_e = 0) = G_G(\tau_e = 0)$, $\dot{G}_E(\tau_e = 0) = \dot{G}_G(\tau_e = 0)$] the transient response becomes more complicated. An additional signal, coming from the configuration in which the probe pulse precedes the pump one, may in principle appear. One finds after a straightforward but lengthy calculation:

$$\begin{aligned} f_E(\tau_e) &= q\,, \\ G_E(\tau,\tau_e) &= Y(\tau_e-\tau)G_{E,0}(\tau) + Y(\tau-\tau_e)G_{E,1}(\tau,\tau_e)\,, \end{aligned}$$

where the function $G_{E,0}(\tau)$ has been defined above and where (in the simplified case, in which $\gamma_E = \gamma_G = \gamma$):

$$G_{E,1}(\tau,\tau_e) = \frac{Y(\tau_e)}{m\Omega_E}\, \exp(-\gamma\tau/2)\Big\{\cos[\Omega_G(\tau_e-\tau)]\sin(\Omega_E\tau_e) - \frac{\Omega_E}{\Omega_G}\sin[\Omega_G(\tau_e-\tau)]\cos(\Omega_E\tau_e)\Big\} \qquad (44)$$

This yields finally:

$$\Delta\sigma^{(\mathrm{I})}(\tau,\tau_e) = n_0 q^2 Y(\tau_e)\exp(-\tau_e/\tau_c)\Big[Y(\tau_e-\tau)\dot{G}_{E,0}(\tau) + Y(\tau-\tau_e)\dot{G}_{E,1}(\tau,\tau_e) - \dot{G}_G(\tau)\Big]\,. \qquad (45)$$

In the Fourier space the behavior of the transient conductivity is determined by the position of the poles. These are defined as the zeroes of the denominator function

$$D_{E,G}(\Omega) = \omega_{E,G}^2 - \Omega^2 + i\Omega\gamma_{E,G}\,, \qquad (46)$$

where Ω is a general frequency variable. One obtains in the strongly perturbed systems [using Eq. (43)]:

$$\Delta\sigma^{(\mathrm{II})}(\omega,\omega_p) = \frac{n_0 q^2}{m}\left[\frac{\omega - i/\tau_c}{\omega_p - i/\tau_c}\,\frac{1}{D_E(\omega - i/\tau_c)} - \frac{\omega-\omega_p}{\omega_p - i/\tau_c}\,\frac{1}{D_G(\omega-\omega_p)}\right] \tag{47}$$

and in the weakly perturbed systems [using (45)]:

$$\Delta\sigma^{(\mathrm{II})}(\omega,\omega_p) = \frac{n_0 q^2}{m}\,\frac{1}{D_E(\omega - i/\tau_c)}\,\frac{\omega - i/\tau_c}{\omega_p - i/\tau_c}\left[1 - \frac{D_E(\omega-\omega_p)}{D_G(\omega-\omega_p)}\right]. \tag{48}$$

The poles of the functions $D_j(\omega - i/\tau_c)$ occur at renormalized eigenfrequencies

$$\omega^2 = \omega_j'^2 \equiv \omega_j^2 + 1/\tau_c^2 + \gamma_j/\tau_c\,, \tag{49}$$

and the poles of $D_j(\omega-\omega_p)$ occur at

$$(\omega-\omega_p)^2 = \omega_j^2\,, \tag{50}$$

where $j = E, G$. Examples of the transient conductivity spectra for several sets of parameters are shown in Figure 5. As there are many possible qualitatively different combinations of the parameters for the harmonic oscillator case we will describe here only the main features of the amplitude spectra. The principal poles of the transient conductivity are clearly visible in Figures 5a,b,e, which correspond to underdamped dynamics. The denominators of Eqs. (47) and (48) determine the poles which have the form of straight lines in the (ω,ω_p) space: $\omega = \pm\omega'_E$, $\omega - \omega_p = \pm\omega_G$, $\omega_p = 0$. The characteristic maxima of the conductivity are then given by intersections of these lines. Thus, one finds three principal maxima in the weakly perturbed case (Figure 5a,b): $[\omega,\omega_p] = [\pm\omega'_E, 0]$, $[\pm\omega_G, 0]$, $[\pm\omega'_E, \pm(\omega'_E - \omega_G)]$, and two principal maxima in the strongly perturbed case [the last one is lacking due to the absence of the product $D_E D_G$ in the denominator of (47)]. The cases $\omega_G > \omega_E$ and $\omega_G < \omega_E$ for the strongly perturbed systems cannot be easily distinguished from each other using the amplitude information only and the knowledge of the phase is required. The increase of damping causes the broadening of the above discussed peaks along ω (case of γ_E), along ω_p (case of τ_c), and along the diagonal $\omega - \omega_p$ (case of γ_G). Note that the common feature of all these spectra (and consequently the characteristic feature of the harmonic oscillator behavior) is the presence of maxima at $\omega_p = 0$ and $\omega \neq 0$.

A 1D inverse Fourier transform yielding the time-resolved THz spectra leads to a complicated expression. This expression simplifies upon considering only the case when the pump pulse precedes the probe, $\tau_p > 0$. One obtains for both weakly and strongly perturbed systems:

$$\Delta\sigma^{(\mathrm{II})}(\omega,\tau_p) \;\propto\; i\exp(-\tau_p/\tau_c) \times \left[\frac{\omega - i/\tau_c}{D_E(\omega - i/\tau_c)} - \frac{\omega - i/\tau_c}{D_G(\omega - i/\tau_c)}\right] \tag{51}$$

The time dependent THz spectrum is thus driven by the exponential decay due to depopulation of the excited level and it shows poles at renormalized eigenfrequencies $\omega'^2_{E,G}$. Concerning 1D experimental scans, analogous conclusions to those deduced in paragraph C can be drawn.

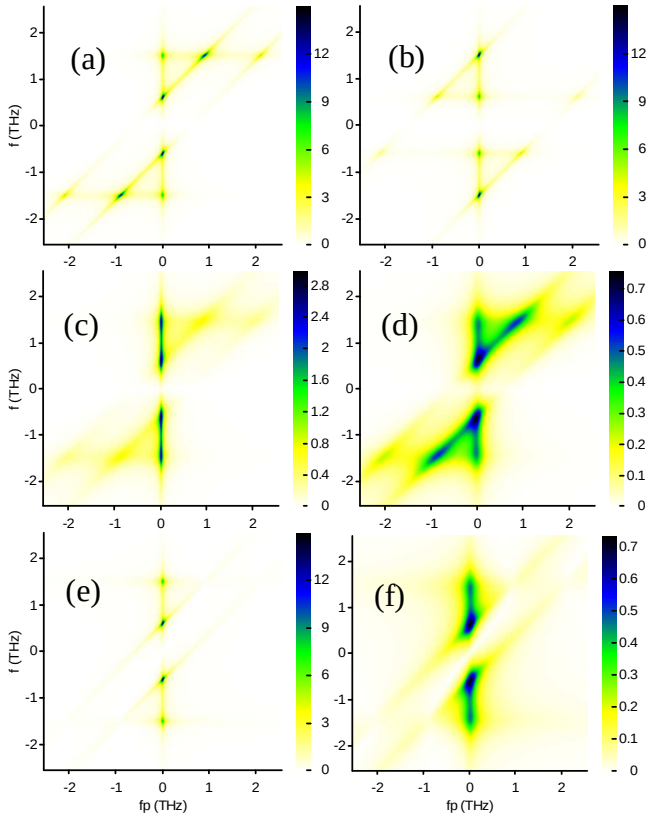

FIG. 5: Simulations of the amplitude of transient 2D conductivity $\Delta\sigma^{(\mathrm{II})}(\omega,\omega_p)$ for harmonic oscillator dynamics. Weakly perturbed case [following (48)]: plots a,b,c, and d; strongly perturbed case (47): plots e and f. Eigenfrequencies of harmonic oscillators: $\omega_E/2\pi = 1.5$ THz and $\omega_G/2\pi = 0.6$ THz (faster motion in the excited state) for all figures except (b) where these values are interchanged (slower motion in the excited state). Dampings ($\gamma_E = \gamma_G = \gamma$) and lifetimes ($\tau_c$): (a,b,e): $\gamma = 0.4\ \mathrm{ps}^{-1}$, $\tau_c = 6$ ps (underdamped, long-lived); (c): $\gamma = 2\mathrm{ps}^{-1}$, $\tau_c = 6$ps (strongly damped, long-lived); (d,f): $\gamma = 2\ \mathrm{ps}^{-1}$, $\tau_c = 1.5$ ps (strongly damped, short-lived).

D. Harmonic oscillators: Relaxation of the coupling constant

In some molecular systems it may happen that the frequency of an oscillatory mode does not change appreciably upon photo-excitation, while, due to spatial charge transfer, the effective charge coupling of the mode with the THz probe field may exhibit some dynamics:

$$m\frac{d^2x}{dt^2} + m\gamma\frac{dx}{dt} + m\omega_0^2 x = f_i E_0(t)\,, \qquad (52)$$

with

$$\begin{aligned} f_G &= q\,, \qquad (53)\\ f_E &= q[1 + Y(\tau_e)(\beta + \alpha\exp(-\tau_e/\tau_b))]\,. \end{aligned}$$

This problem can be also solved analytically. One then finds the poles at $[\omega, \omega_p] = [\pm\omega_0', 0]$, $[\pm\omega_0, 0]$, where analogously to Eq. (49):

$$\omega_0'^2 = \omega_0^2 + 1/\tau_b^2 + \gamma/\tau_b\,. \qquad (54)$$

It is also possible to combine this problem with that discussed in the preceding paragraph, i.e., to solve a simultaneous step-like change of the eigenfrequency and of the effective charge.

E. Excitation of an anharmonic vibrational mode

In this paragraph we continue to deal with two oscillatory modes. We refer here to the case when we can still describe the ground-state oscillator within the harmonic approximation (small probing field limit). In a large number of systems, though, the potential minimum of the excited state is shifted with respect to that of the ground state. The initial position of the excited-state oscillator thus can be far from equilibrium. This means that the mode after photo-excitation can exhibit a highly anharmonic motion.

This case cannot be solved analytically and requires a slightly deeper insight into the problem than that used in the previous model cases. This treatment will also allow us to see more clearly the connection between the phenomenological models and molecular dynamics simulations. Our approach is based on a numerical solution of equations of motion for a particle with coordinate X in the potential $V(X, \tau_e)$. In the excited state the equation for the trajectory $X_{E,0}$ without the probing THz field reads:

$$m\frac{d^2X_{E,0}}{dt^2} + m\gamma\frac{dX_{E,0}}{dt} + \frac{\partial V(X_{E,0}, \tau_e)}{\partial X_{E,0}} = 0\,. \qquad (55)$$

The presence of a probing field changes the trajectory to $X_E = X_{E,0} + x_E$. Note that in paragraph C we did not need to introduce the variables X_E and $X_{E,0}$ and that we wrote directly the equation of motion for the field-induced deviation x_E. As we show later, this is possible for harmonic motions, however, the present case requires a more general approach. The equation of motion with the probing field can be then written as:

$$m\frac{d^2X_E}{dt^2} + m\gamma\frac{dX_E}{dt} + \frac{\partial V(X_E, \tau_e)}{\partial X_E} = q\delta(t)\,. \qquad (56)$$

Subtracting (55) from (56) and neglecting higher-order terms in x_E one obtains:

$$m\frac{d^2x_E}{dt^2} + m\gamma\frac{dx_E}{dt} + \frac{\partial^2 V(X_{E,0}, \tau_e)}{\partial X_{E,0}^2}x_E = q\delta(t)\,. \qquad (57)$$

The most important result is that this equation is linear in x_E and that it contains only the potential at the trajectory evaluated without the probing field. Here we can see a link to molecular dynamics simulations, namely to the method of instantaneous normal modes (INM). These simulations yield trajectories $X_{E,0}$ and the spectral distribution of normal modes along these trajectories. This is encoded in the potential term in Eq. (57). The INM approach represents a viable alternative to direct molecular dynamics calculations of spectra, discussed in Ref. 18. Adopting the INM approach allows suppressing the inherent statistical noise of the simulations. The price for involving an instantaneous harmonic picture is the limited applicability to short-time dynamics only, particularly for strongly anharmonic systems. The experiment gives access to x_E controlled by the potential term. The response of the system is calculated by solving Eqs. (55) and (57) for a particular potential.

The ground state is treated analogously. However, for a harmonic potential, Eq. (57) is independent of $X_{E,0}$: this directly leads to the treatment of the ground state developed in paragraph C.

Examples of the anharmonic behavior obtained by the above numerical calculation are shown in Figure 6. The excitation pathway (1) corresponds to the harmonic approximation: the corresponding plot of the transient conductivity is equivalent to that shown in Figure 5a. The increasing anharmonicity of the motion (excitation pathways 2–5) then leads to the disappearance of conductivity maxima at $\omega_p = 0$ and to the enhancement and broadening of the maxima at $\omega_p, \omega \neq 0$. A strong presence of such maxima is the fingerprint of the anharmonicity of the probed dynamics in the excited state.

IV. CONCLUSION

We have described the methodology of the optical pump—THz probe experiments and the procedure of the data treatment for an analytical extraction of the two-dimensional transient conductivity, mapping out the ultrafast evolution of far-infrared polar spectra. We have derived expressions for the transient conductivity in model cases of free charges and of bound ones in a harmonic and anharmonic potentials. The shape of the

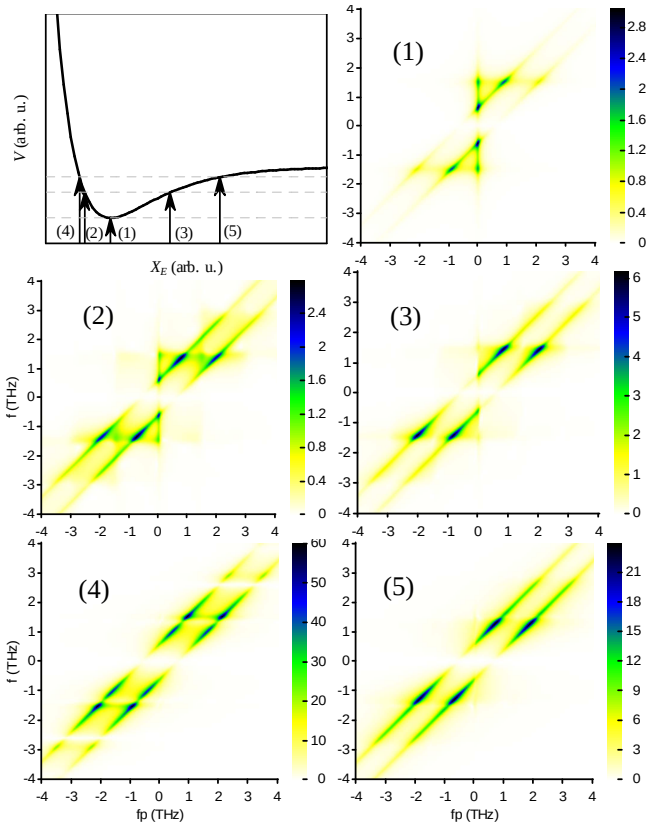

FIG. 6: Simulations of the amplitude of transient 2D conductivity $\Delta\sigma^{(\mathrm{II})}(\omega,\omega_p)$ for anharmonic oscillator dynamics. The ground state is a harmonic potential with $\omega_G/2\pi = 0.6$ THz. The potential of the excited state (we use Morse potential model)[28] is shown in the uppermost left plot along with the excitation pathways (1–5) that were used for the calculation of the conductivity in the remaining plots; the resonant frequency of its harmonic part is $\omega_E/2\pi = 1.5$ THz.

amplitude spectra presents characteristic fingerprints allowing a clear distinction between localized and delocalized state dynamics. The possibility of spectra fitting by a complex 2D function in principle enables a fine adjustment of model parameters and an independent check of the correctness of the experimental results.

The approach developed in this paper allowed us to discuss the relevance of the dynamical information that can be extracted from one-dimensional time delay scans. In particular, we have shown that, in such experiments, the data obtained with short pump–probe delays (shorter than THz pulse length) can lead to inherent artifacts depending on the particular THz field profile.

Acknowledgments

Financial support from the Ministry of Education of the Czech Republic (project No. LN00A032) is gratefully acknowledged.

* Electronic address: `kuzelp@fzu.cz`

[1] M. C. Nuss and J. Orenstein, *Terahertz Time-Domain Spectroscopy*, vol. Chap. 2 of *Millimeter and Submillimeter Wave Spectroscopy of Solids* (Springer-Verlag Berlin Heidelberg, 1998).
[2] D. Mittleman, *Sensing with Terahertz Radiation* (Springer-Verlag, Berlin, 2003).
[3] C. A. Schmuttenmaer, Chem. Rev. **104**, 1759 (2004).
[4] J. T. Kindt and C. A. Schmuttenmaer, J. Chem. Phys. **110**, 8589 (1999).
[5] H. Němec, F. Kadlec, and P. Kužel, J. Chem. Phys. **117**, 8454 (2002).
[6] M. C. Nuss, D. H. Auston, and F. Capasso, Phys. Rev. Lett. **58**, 2355 (1987).
[7] B. I. Greene, J. F. Federici, D. R. Dykaar, A. F. J. Levi, and L. Pfeiffer, Opt. Lett. **16**, 48 (1991).
[8] M. Schall and P. U. Jepsen, Opt. Lett. **25**, 13 (2000).
[9] M. C. Beard, G. M. Turner, and C. A. Schmuttenmaer, Phys. Rev. B **62**, 15764 (2000).
[10] M. C. Beard, G. M. Turner, and C. A. Schmuttenmaer, J. Appl. Phys. **90**, 5915 (2001).
[11] R. D. Averitt, G. Rodriguez, J. L. W. Siders, S. A. Trugman, and A. J. Taylor, J. Opt. Soc. Am. B **17**, 327 (2000).
[12] J. Demsar, R. D. Averitt, A. J. Taylor, V. V. Kabanov, W. N. Kang, H. J. Kim, E. Choi, and S. Lee, Phys. Rev. Lett. **91**, 267002 (2003).
[13] E. Knoesel, M. Bonn, J. Shan, and T. F. Heinz, Phys. Rev. Lett. **86**, 340 (2001).
[14] G. Haran, W.-D. Sun, K. Wynne, and R. M. Hochstrasser, Chem. Phys. Lett. **274**, 365 (1997).
[15] R. McElroy and K. Wynne, Phys. Rev. Lett. **79**, 3078 (1997).
[16] M. C. Beard and C. A. Schmuttenmaer, J. Chem. Phys. **114**, 2903 (2001).
[17] M. C. Beard, G. M. Turner, and C. A. Schmuttenmaer, ACS Symposium Series 820 (ACS, Washington DC, 2002).
[18] F. Kadlec, C. Kadlec, P. Kužel, P. Slavíček, and P. Jungwirth, J. Chem. Phys. **120**, 912 (2004).
[19] H. Němec, F. Kadlec, C. Kadlec, P. Kužel, and P. Jungwirth, J. Chem. Phys. (2004), next paper in this issue.

[20] S. Gupta, M. Y. Frankel, J. A. Valdmanis, J. F. Whitaker, G. A. Mourou, F. W. Smith, and A. R.Calawa, Appl. Phys. Lett. **59**, 3276 (1991).
[21] F. Doany, D. Grischkowsky, and C.-C. Chi, Appl. Phys. Lett. **50**, 460 (1987).
[22] S. Gupta, J. F. Whitaker, and G. A. Mourou, IEEE J. Quantum Electron. **28**, 2464 (1992).
[23] P. U. Jepsen, R. H. Jacobsen, and S. R. Keiding, J. Opt. Soc. Am. B **13**, 2424 (1996).
[24] G. Segschneider, F. Jacob, T. Löffler, H. G. Roskos, S. Tautz, P. Kiesel, and G. Döhler, Phys. Rev. B **65**, 125205 (2002).
[25] F. A. Hegman, R. R. Tykwinsky, K. P. H. Lui, J. E. Bullock, and J. E. Anthony, Phys. Rev. Lett. **89**, 227403 (2002).
[26] S. S. Prabhu, S. E. Ralph, M. R. Melloch, and E. S. Harmon, Appl. Phys. Lett. **70**, 2419 (1997).
[27] P. Kužel, M. A. Khazan, and J. Kroupa, J. Opt. Soc. Am. B **16**, 1795 (1999).
[28] J. P. Dahl and M. Springborg, J. Chem. Phys. **88**, 4535 (1988).